

To be published in Applied Optics:

Title: THz Spectroscopy with a Holographic Fourier Transform Spectrometer Plus Array Detector Using Coherent Synchrotron Radiation

Authors: N. Agladze, J. Klopf, G. Williams, and A. Sievers

Accepted: 5 May 2010

Posted: 14 May 2010

Doc. ID: 125306



Report Documentation Page				Form Approved OMB No. 0704-0188	
Public reporting burden for the collection of information is estimated to average 1 hour per response, including the time for reviewing instructions, searching existing data sources, gathering and maintaining the data needed, and completing and reviewing the collection of information. Send comments regarding this burden estimate or any other aspect of this collection of information, including suggestions for reducing this burden, to Washington Headquarters Services, Directorate for Information Operations and Reports, 1215 Jefferson Davis Highway, Suite 1204, Arlington VA 22202-4302. Respondents should be aware that notwithstanding any other provision of law, no person shall be subject to a penalty for failing to comply with a collection of information if it does not display a currently valid OMB control number.					
1. REPORT DATE 2010		2. REPORT TYPE		3. DATES COVERED 00-00-2010 to 00-00-2010	
4. TITLE AND SUBTITLE THz Spectroscopy with a Holographic Fourier Transform Spectrometer Plus Array Detector Using Coherent Synchrotron Radiation				5a. CONTRACT NUMBER	
				5b. GRANT NUMBER	
				5c. PROGRAM ELEMENT NUMBER	
6. AUTHOR(S)				5d. PROJECT NUMBER	
				5e. TASK NUMBER	
				5f. WORK UNIT NUMBER	
7. PERFORMING ORGANIZATION NAME(S) AND ADDRESS(ES) Laboratory of Atomic and Solid State Physics, Cornell University, Ithaca, NY, 14853-2501				8. PERFORMING ORGANIZATION REPORT NUMBER	
9. SPONSORING/MONITORING AGENCY NAME(S) AND ADDRESS(ES)				10. SPONSOR/MONITOR'S ACRONYM(S)	
				11. SPONSOR/MONITOR'S REPORT NUMBER(S)	
12. DISTRIBUTION/AVAILABILITY STATEMENT Approved for public release; distribution unlimited					
13. SUPPLEMENTARY NOTES					
14. ABSTRACT					
15. SUBJECT TERMS					
16. SECURITY CLASSIFICATION OF:			17. LIMITATION OF ABSTRACT Same as Report (SAR)	18. NUMBER OF PAGES 22	19a. NAME OF RESPONSIBLE PERSON
a. REPORT unclassified	b. ABSTRACT unclassified	c. THIS PAGE unclassified			

THz Spectroscopy with a Holographic Fourier Transform Spectrometer Plus Array Detector Using Coherent Synchrotron Radiation

N. I. Agladze,¹ J. M. Klopf,² G. P. Williams,² and A. J. Sievers^{1,*}

*¹Laboratory of Atomic and Solid State Physics, Cornell University
Ithaca, NY 14853-2501, USA*

*²Free Electron Laser Facility, Jefferson Lab, 12000 Jefferson Avenue,
Newport News, VA 23606, USA*

**Corresponding author: sievers@ccmr.cornell.edu*

Using coherent THz synchrotron radiation a holographic Fourier transform spectrometer coupled to an array detector was tested experimentally to determine its viability as a spectral device. Somewhat surprisingly the overall performance strongly depends on the absorptivity of the birefringent lithium tantalate pixels in the array detector.

OCIS codes: 120.6200, 300.6270, 260.3160, 300.6300.

With the development of coherent broadband THz synchrotron sources based on the radiation produced by short bunches of electrons in storage rings[1], interest has developed in the appropriate spectroscopic instrumentation for bunch length measurements[2, 3], which correspond to the sub-picosecond time-scale. In addition to single shot spectroscopy measurements there is also interest in using this mm and submillimeter coherent wave radiation signature from the bunch for its structural analysis. Spectroscopic measurement of the bunch length by means of its coherent radiation signature becomes technically easier as the bunch gets shorter in length since the resulting radiation extends over a larger frequency interval. The determination of the bunch form factor using this technique has been described in some detail[4-8].

A candidate instrument for the types of study just outlined is a holographic Fourier transform spectrometer (HFTS), which has no moving parts and produces an interferogram in the spatial, not in the time domain. Thanks to its high throughput, HFTS have found use in the remote and time dependent sensing areas, where they outperform even multichannel spectrographs[9]. The extremely broad spectral coverage of an HFTS would be particularly beneficial in the THz region where a diffraction grating cannot be used without elaborate optics for filtering out higher diffraction orders. But the large interference angle required for a THz HFTS makes associated field aberrations too large for a realistic size of the array detector. This difficulty has been resolved by dividing the Fourier optics into two halves with a tilt interferometer design [10]. Here we present experimental tests of this new THz HFTS instrument using the coherent synchrotron radiation produced in the energy recovery linac of the free electron laser facility at Jefferson Laboratory.

A three dimensional schematic of the THz HFTS optical design is shown in Fig. 1. The fore optics consisting of a 45° off-axis parabolic mirror accepts the collimated THz radiation. The intermediate focus is formed slightly behind a wire grid beamsplitter, which also serves as the field angle-limiting aperture. The motor driven shutter in each arm provides the means to measure the intensity in each of the interferometer arms. The two tilted mirrors direct the beams towards the 30° off-axis parabolic mirrors, which serve as the mirror analog of the Fourier transform lens. Finally the collimated beams converge on the array detector located with its plane perpendicular to the axial beams bisector. An additional wire grid polarizer is located next to the detector (not shown) in order to mix the orthogonal polarizations propagating along the interferometer arms. Assuming the amplitude transmission and reflection coefficients are τ and $1 - \tau$ at the beamsplitter for a specific polarization analyzed by the detector, then the intensity produced in the detector plane (xy) by beams along the axial directions is given by the following relation [10]

$$I(x, y) = \int_0^\infty I^0(\sigma, x, y) \left\{ \tau^2 + (1 - \tau)^2 + 2\tau(1 - \tau) \cos[(2\pi\sigma y)2\sin(\alpha/2)] \right\} B(\sigma) d\sigma, \quad (1)$$

where $I^0(\sigma, x, y)$ is the intensity at frequency $\sigma \equiv 1/\lambda$ (λ is the wavelength). The factor $2\sin(\alpha/2)$ in the cosine argument determines the scale of the interference pattern. This scaling factor determines the spectral resolution and the high frequency cutoff of the instrument for a given size and pixel dimension of the array detector. The only commercial array detector available today for the THz region is the Pyrocam III, which was used in these experiments. Its sensitivity is sufficiently low that this instrument could not be tested with incoherent sources of THz radiation such as a globar or mercury arc. All experimental tests of the new spectrometer were performed using coherent THz synchrotron radiation.

Synchrotron radiation produced by short electron bunches in one of the bending magnets of the Jefferson Lab Free Electron Laser facility [11] was delivered through a vacuum optical transmission line [12] into a class 4 laser shielded laboratory. Figure 2 shows the actual arrangement. After the diamond exit window (1) the THz radiation propagated in air and it is collimated with a 90° parabolic reflector (2). The original horizontal polarization of the synchrotron radiation after reflections in the transfer line appeared at the optical table at a small angle from the vertical direction. (It is referred to as horizontal in the following.) For measurements of transmission spectra an intermediate focus was created between a pair of additional 90° parabolic mirrors (3) and (4). The tilt interferometer (7) is located in the collimated beam and the array detector (8) is installed on a translation stage so that the center burst of the static interference pattern produced by the interferometer can be positioned at any pixel of the array.

In order to compensate for the non-uniform illumination of the detector area the following calibration procedure was used. Three separate measurements were performed for various positions of the shutters blocking the beam in each arm of the interferometer (see Fig. 1). First, the background intensity distribution $I_0(x, y)$ in the array was measured with both shutters closed. Then two intensities $I_1(x, y)$ and $I_2(x, y)$ were measured for shutters blocking only one of the interferometer arms. These distributions $I_1(x, y) - I_0(x, y)$ and $I_2(x, y) - I_0(x, y)$, where the scattered parasitic light is subtracted from each arm of the interferometer, were added and normalized to give the correction factor $k(x, y)$ between 0 and 1. The corrected intensity distribution $I_c(x, y)$ was calculated from the signal $I(x, y)$ with both shutters opened according to the following relation

$$I_c(x,y)=[I(x,y)-I_0(x,y)]/k(x,y) \quad (2)$$

The same correction factors were used for the reference and for the sample spectra during subsequent transmission measurements. This procedure ignores any frequency dependence of the beamsplitter efficiency and assumes that the intensity distributions produced by the two interferometer arms differ only by a constant factor. Generally the latter point is not true for a polarizing beamsplitter with different intensity distributions for horizontal and vertical polarizations of the synchrotron radiation. In order to avoid this problem an additional polarizer transmitting only horizontal polarization was installed before the interferometer.

Measurements were performed in the quasi-continuous mode using the internal chopper of the Pyrocam detector to interrupt the incoming THz beams at 48 Hz. A laptop computer running LabVIEW software controlled the operation of the shutters and of the array detector. Spectra were calculated and displayed in real time. Two positions were used for the center burst of the spatial interferograms. When the maximum possible resolution was desired it was located at the 10th pixel, and when a better phase correction was required it was located at the 20th pixel from the edge. The Pyrocam III detector has 124 X 124 square pixels with the pitch 100 μm so the resulting spectral resolution is $1.2 - 1.3 \text{ cm}^{-1}$, with a maximum non-aliased frequency of 114 cm^{-1} .

Examples of corrected static interference patterns and corresponding calculated spectra are shown in Fig. 3. Notable are the periodic oscillations in the spectra. These measurements were performed with the following parameters of the energy recovery linac: current 1 mA, bunch charge 100 pC, repetition rate 9.36 MHz, beam energy 114.65 MeV. The Pyrocam III accumulation time was 1 second. Detuning of the bunch energy by changing the gradient field in

the RF cavities varied the electron bunch length. The sharpest center burst is observed for the -70 keV to -140 keV detuning, hence the narrowest electron bunch is observed at this beam energy.

In order to determine the spectral response of the array detector it was used together with a scanning Michelson interferometer to analyze the same synchrotron radiation. Both the scanning Michelson and the HFTS spectral results are shown in Fig. 4 with dot-dash and solid lines, respectively. Apart from a difference in resolution the two spectra are quite similar confirming that the non-uniform spectral response of the THz HFTS measurement is due to the detector array. For an additional comparison the same spectral region was measured with the Golay cell in the scanning Michelson interferometer (dashed line in Fig. 4). Crossed wire grid polarizers were used to attenuate the radiation to the level acceptable for the Golay cell. The most probable explanation of the spectral non-uniform characteristics of the array detector is the production of a channel spectrum in its pixels. The measured period 15 cm^{-1} corresponds to a $50 \text{ }\mu\text{m}$ thickness for the lithium tantalate used in the detector elements. Note that similar non-uniform spectral response due to a channel spectrum has also been reported in some single element pyroelectric detectors [8].

To examine the high frequency characteristics of the THz HFTS a transmission spectrum of a band pass THz filter (QMC Instruments) was measured as well. The results for the HFTS are compared with those from a lamellar interferometer with a Golay detector in Fig. 5. The angular distribution of the coherent synchrotron radiation is wavelength dependent due to the electron beam vacuum chamber screening effects[13]. For the effective focal length of 10 cm used here the angular distribution is sufficiently narrow at the filter transmission maximum (28 cm^{-1}) so that the collimated beam did not cover the whole area of the array detector at this frequency. This

resulted in the effective degradation of the spectral resolution of the HFTS but the general shape of the band pass filter spectrum is similar for both kinds of spectrometers.

For a more detailed spectral test of the HFTS plus array detector the channel spectrum of a silicon slab was also measured and compared with that determined from a lamellar interferometer plus Golay measurement. The results are shown in Fig. 6, where a clear difference between the two spectra is evident. In order to understand this difference first the parameters for the standard lamellar spectrum are determined. The silicon wafer of thickness $d = 401 \mu\text{m}$ has only one side polished; the other surface is rough with a characteristic grain size $\sim 50 \mu\text{m}$, determined with the aid of an optical microscope, so only a two pass interference spectrum is expected. The equation that describes the silicon wafer spectrum fit with one two-pass interference beam is

$$T(\sigma) = \frac{16n^2}{(n+1)^4} \left[1 + \frac{(n-1)^4}{(n+1)^4} + 2 \frac{(n-1)^2}{(n+1)^2} \cos(4\pi\sigma nd + \varphi) \right], \quad (3)$$

where the constant phase angle φ has been included to take account of the change produced by the free carrier contribution at frequencies below this range. The exact properties of the rough wafer surface are not included in this model expression. Fitting Eq. (3) to the lamellar spectrum gives $n = 3.43 \pm 0.03$ and $\varphi = -1.2 \pm 0.4$ for the silicon refractive index and the phase at THz frequencies. This spectrum is represented by the dotted trace in Fig. (6). Clearly the modulation occurs at the correct frequency intervals but the experimentally measured amplitude is greatly reduced due to the surface roughness.

Next consider the irregular frequency shifts that appear in the THz HFTS spectrum. These frequency shifts are consistent with a beating between two different silicon channel

spectra. One spectrum is described by Eq. (3) and the second one has a different scale resulting from the beams incident on the array at a slightly different angle. The result is Eq. (4).

$$T(\sigma) = A + C \{ D \cos(4\pi\sigma nd + \varphi) + (1 - D) \cos[4\pi\sigma nd \sin(\alpha/2) / \sin(\alpha/2 + \delta) + \varphi] \} \quad (4)$$

where δ is the change of the angle transmitted through the pixels, D describes the relative strength of the beating spectra, $\alpha = 24.4^\circ$ is the tilt interferometer designed angle. Parameters A and C account for the non-ideal reflections from the rough silicon surface. The result of the fit using Eq. (4) is shown in Fig. 7. The following parameters were found to be optimal. $A = 0.47 \pm 0.01$; $C = 0.28 \pm 0.04$; $D = 0.58 \pm 0.02$; $\delta = 1.67^\circ \pm 0.04^\circ$. The poor agreement near 15 cm^{-1} is due to the large error in the transmission spectrum as a result of the small intensity at this frequency, as shown in Fig. 4. It should be noted that neither the angular distribution of the radiation at the silicon sample nor the angular dependence of the scaling factor in the THz HFTS can generate a second scaling factor.

How can one account for an extra angle that appears to be necessary? It is clear from Fig. 4 that multiple reflections occur within the pixel array demonstrating that the THz radiation passes through the lithium tantalate pixels. Due to the birefringence of the pixel material and polarization mixing inside the detector structure a beam coming from an interferometer arm can split into two beams with a few degrees difference. After reflection from the back metal plate of the array these beams will fall on the pixels from the backside again and will produce a rescaled interferogram component. This change in angle will result in scaling factors $2 \sin(\alpha/2)$ and $2 \sin(\alpha/2 + \delta)$ for the incident and reflected beam paths, respectively. The fitted angle $\delta = 1.67^\circ$ is compatible with the expected lithium tantalate birefringence effect. This simple model is not a substitute for the rigorous treatment taking into account the near field effects in the real 3D array

detector structure. Such a treatment is not possible because of proprietary restrictions on the array construction; however, the model illustrates what happens when the array is not properly designed for holographic spectral measurements at THz frequencies.

To optimize this spectroscopic system at least two changes in the array detector fabrication are recommended. The pixels should be vacuum impedance matched in the THz region to increase the sensitivity and an efficient absorber should be placed behind the pixels to avoid complications due to back reflections of the beams. Since the pixel spacing in the array sets the shortest wavelength limit of the HFTS the pixel size should be reduced so that a broader spectral range can be covered.

Summarizing, the experimental test of the holographic FTS for the THz region demonstrate the following.

(1) A new spectrometer design for the THz, the HFTS built around the tilt interferometer, using an array detector and coherent synchrotron radiation has been demonstrated.

(2) A qualitative characterization of the electron bunch length with the new instrument is shown.

(3) These experimental tests of the new spectrometer demonstrate its viability as a spectral device and reveal that its performance is strongly dependent on the details of the array detector construction.

Acknowledgments

This work was supported by DOE-DE-FG02-04ER46154 and by NSF-DMR-0906491. Use of facilities of the Cornell Center for Material Research (NSF-DMR-0520404) is also acknowledged. Activities at Jefferson Lab were supported by the Office of Naval Research, the

Army Night Vision Lab, Advanced Energy Systems, and the U.S. DOE under contract No. DE-AC05-06OR23177.

Published by
OSA

References

1. T. Nakazato, M. Oyamada, N. Niimura, S. Urasawa, O. Konno, A. Kagaya, R. Kato, T. Kamiyama, Y. Torizuka, T. Nanba, Y. Kondo, Y. Shibata, K. Ishi, T. Oshak, and M. Ikezawa, "Observation of Coherent Synchrotron Radiation," *Phys. Rev. Lett.* **63**, 1245 (1989).
2. G. L. Carr, M. C. Martin, W. R. McKinney, J. Jordan, G. R. Neil, and G. P. Williams, "High-power terahertz radiation from relativistic electrons," *Nature* **420**, 153-156 (2002).
3. G. P. Williams, "Filling the THz gap - high power sources and applications," *Rep. Prog. Phys.* **69**, 301-326 (2006).
4. Y. Shibata, T. Takahashi, T. Kanai, K. Ishi, M. Ikezawa, J. Ohkuma, S. Okuda, and T. Okada, "Diagnostics of an electron beam of a linear accelerator using coherent transition radiation," *Phys. Rev. E* **50**, 1479-1484 (1994).
5. R. Lai and A. J. Sievers, "On using the coherent far IR radiation produced by a charged-particle bunch to determine its shape .1. Analysis," *Nucl. Instrum. Methods Phys. Res. A* **397**, 221-231 (1997).
6. G. Schneider, M. G. Billing, R. Lai, and A. J. Sievers, "Comparison of electron bunch asymmetry as measured by energy analysis and coherent transition radiation," *Phys. Rev. E* **56**, R3780-R3783 (1997).
7. T. Watanabe, J. Sugahara, T. Yoshimatsu, S. Sasaki, Y. Sugiyama, K. Ishi, Y. Shibata, Y. Kondo, K. Yoshii, T. Ueda, and M. Uesaka, "Overall comparison of subpicosecond electron beam diagnostics by the polychromator, the interferometer and the femtosecond streak camera," *Nuclear Inst. and Methods Phys. Res. A* **480**, 315-327 (2002).

8. D. Mihalcea, C. L. Bohn, U. Happek, and P. Piot, "Longitudinal electron bunch diagnostics using coherent transition radiation," *Phys. Rev. ST Accel. Beams* **9**, 0828011-0828017 (2006).
9. N. I. Agladze and A. J. Sievers, "Miniaturization of holographic Fourier-transform spectrometers," *Appl. Opt.* **43**, 6568-6579 (2004).
10. N. I. Agladze and A. J. Sievers, "Holographic Fourier transform spectrometer for terahertz region," *Opt. Lett.* **35**, 664-666 (2010).
11. G. R. Neil, C. Behre, S. V. Benson, M. Bevins, G. Biallas, J. Boyce, J. Coleman, L. A. Dillon-Townes, D. Douglas, H. F. Dylla, R. Evans, A. Grippo, D. Gruber, J. Gubeli, D. Hardy, C. Hernandez-Garcia, K. Jordan, M. J. Kelley, L. Merminga, J. Mammosser, W. Moore, N. Nishimori, E. Pozdeyev, J. Preble, R. Rimmer, M. Shinn, T. Siggins, C. Tennant, R. Walker, G. P. Williams, and S. Zhang, "The JLab high power ERL light source," *Nucl. Instrum. Methods Phys. Res., Sect. A* **557**, 9-15 (2006).
12. J. M. Klopff, A. Greer, J. Gubeli, G. R. Neil, M. Shinn, T. Siggins, D. Waldman, G. P. Williams, A. Todd, V. Christina, and O. Chubar, "The Jefferson Lab high power THz user facility," *Nucl. Instrum. Methods Phys. Res., Sect. A* **582**, 114-116 (2007).
13. S. Kheifets and B. Zotter, "Shielding Effects on Coherent Synchrotron Radiation," in *Micro Bunches Workshop*, E. B. Blum, M. Dienes, and J. B. Murphy, eds. (AIP, Woodbury, 1996), p. 424.

Figure Captions

Figure 1. Optical setup of the tilt interferometer based holographic FTS. (1) – fore optics (45° off-axis parabolic mirror); (2) – beamsplitter; (3,4) – shutters; (5,6) – out-of-plane tilted mirrors; (7,8) – two halves of the split Fourier transform system (30° off-axis parabolic mirrors); (9) – the array detector.

Figure 2. Experimental setup at JLab for testing the THz HFTS. Foreground: The THz radiation is delivered from the accelerator through the vacuum transfer line and is focused on the output diamond window (1). The white line identifies the THz radiation optical path. It is collimated by the parabolic reflector (2). An intermediate focus for sample transmission measurements is formed between the two parabolic reflectors (3) and (4). Mirror (5) sends the collimated beam to the interferometer (7). The interference pattern is analyzed with the pyroelectric array detector (8). Background: A removable mirror (6) is used to send the THz beam to a separate experimental setup (9).

Figure 3. Coherent synchrotron radiation interference patterns for different electron bunch lengths and corresponding coherent synchrotron spectra. The larger the frequency interval of the spectrum the shorter is the bunch. The narrowest bunches occur when the gradient field in the RF cavities is between -70 keV and -140 keV. The Pyrocam array has a highly non-uniform spectral response due to the channel spectrum produced in the elements.

Figure 4. Comparison of coherent synchrotron spectra measured with a scanning Michelson interferometer and for the THz HFTS. Solid line: THz HFTS; dot-dash line: Michelson interferometer with the same detector; dashed line: Michelson interferometer with a Golay cell.

Figure 5. Transmission spectrum of a THz band pass filter (QMC Instruments). Solid line: spectrum measured with THz HFTS; dashed line: spectrum measured with a lamellar scanning FTS.

Figure 6. Transmission spectrum of a silicon wafer. Solid line: spectrum measured by the THz HFTS; dashed line: channel spectrum measured with a lamellar scanning FTS; dotted line: the lamellar spectrum fit using Eq. 3. The Si surface roughness reduces the modulation amplitude.

Figure 7. THz HFTS transmission spectrum of the silicon wafer compared with the two-channel model. Solid line: HFTS transmission spectrum; dashed line: fit to the superposition of two channel spectra with two different scales, using Eq. 4.

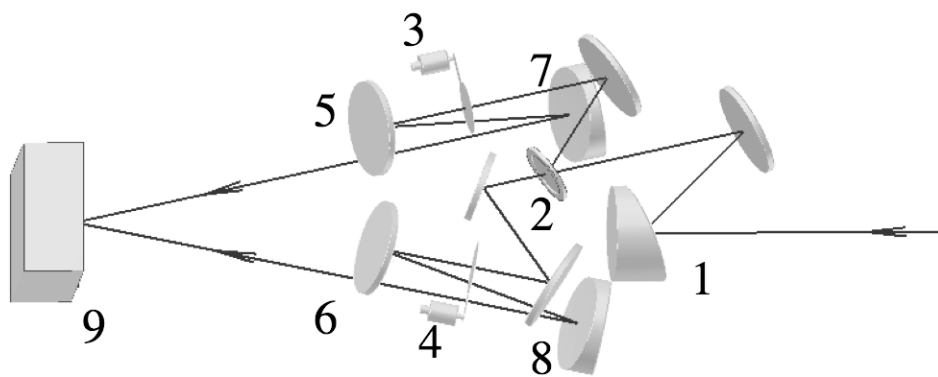


Figure 1.

Published by

OSA

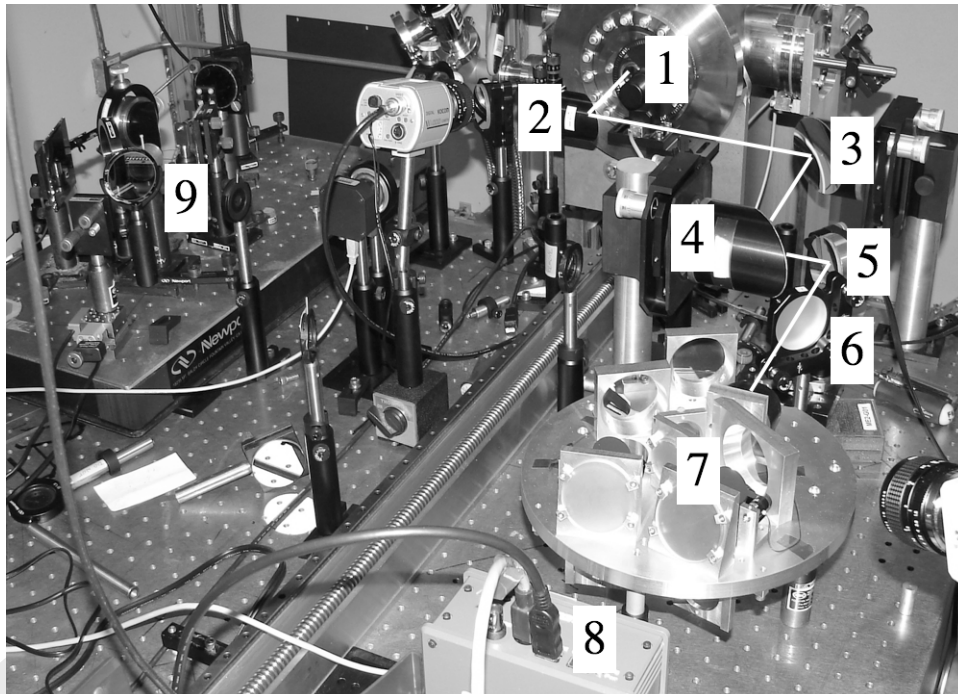


Figure 2.

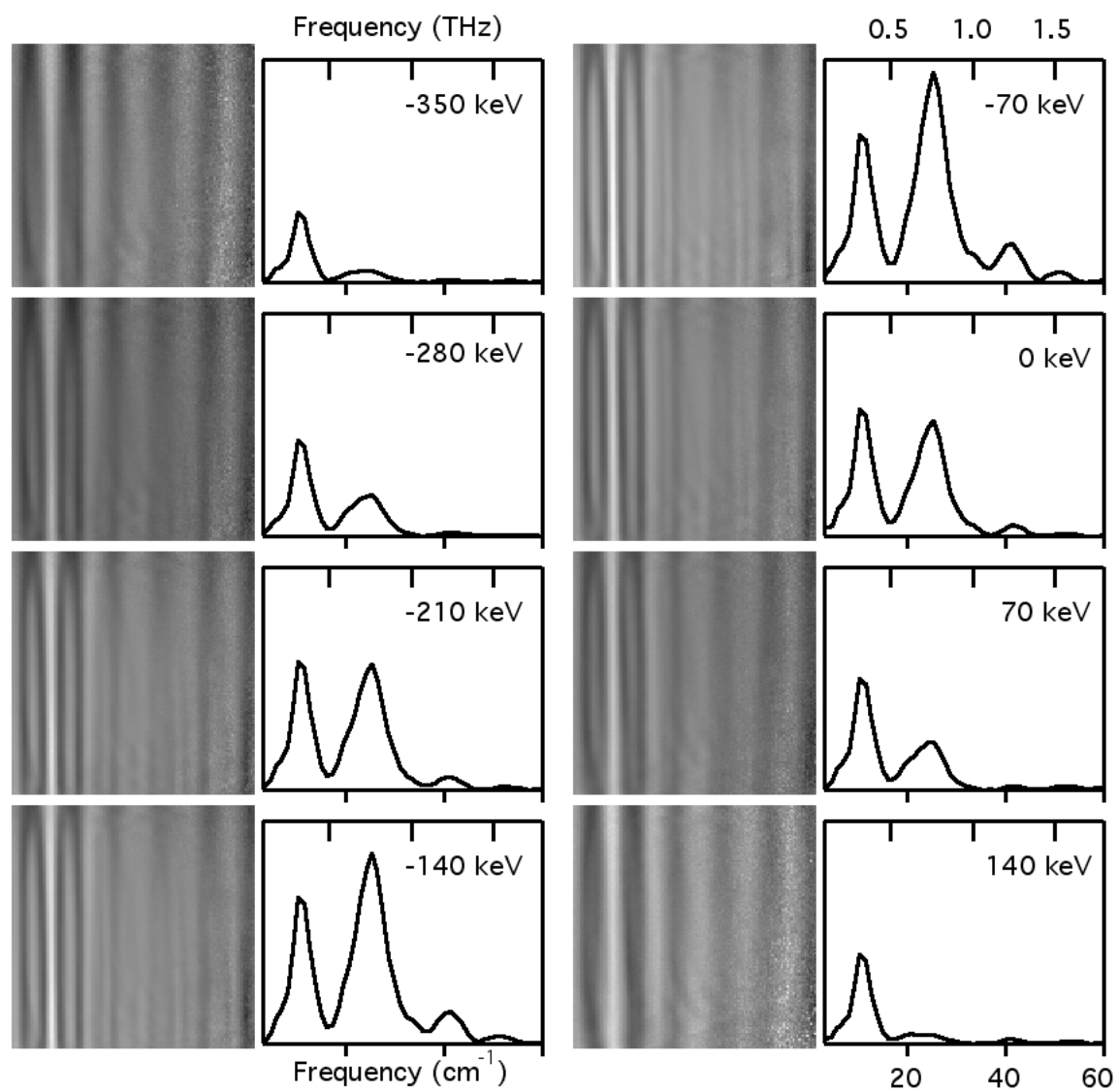


Figure 3.

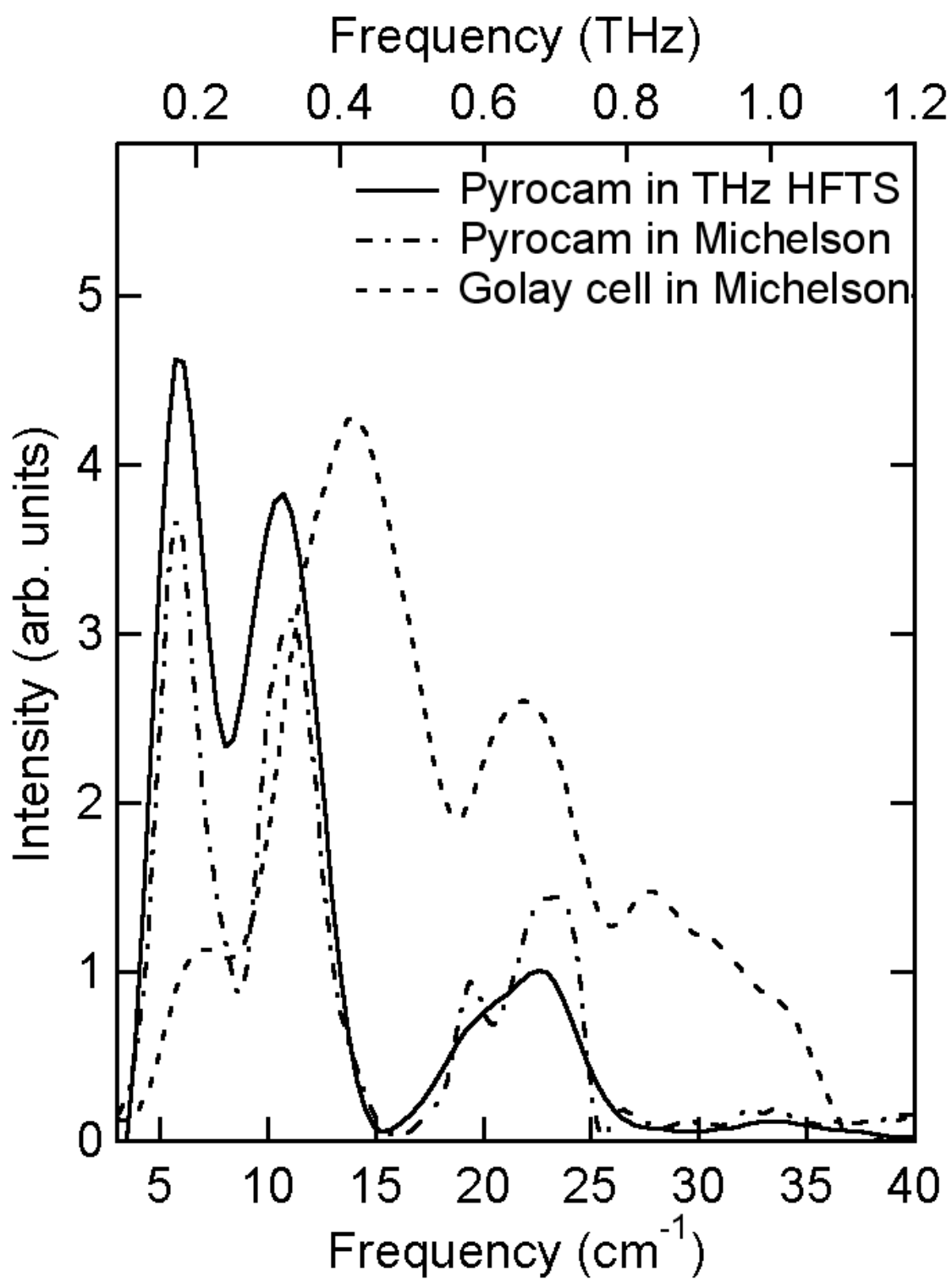


Figure 4.

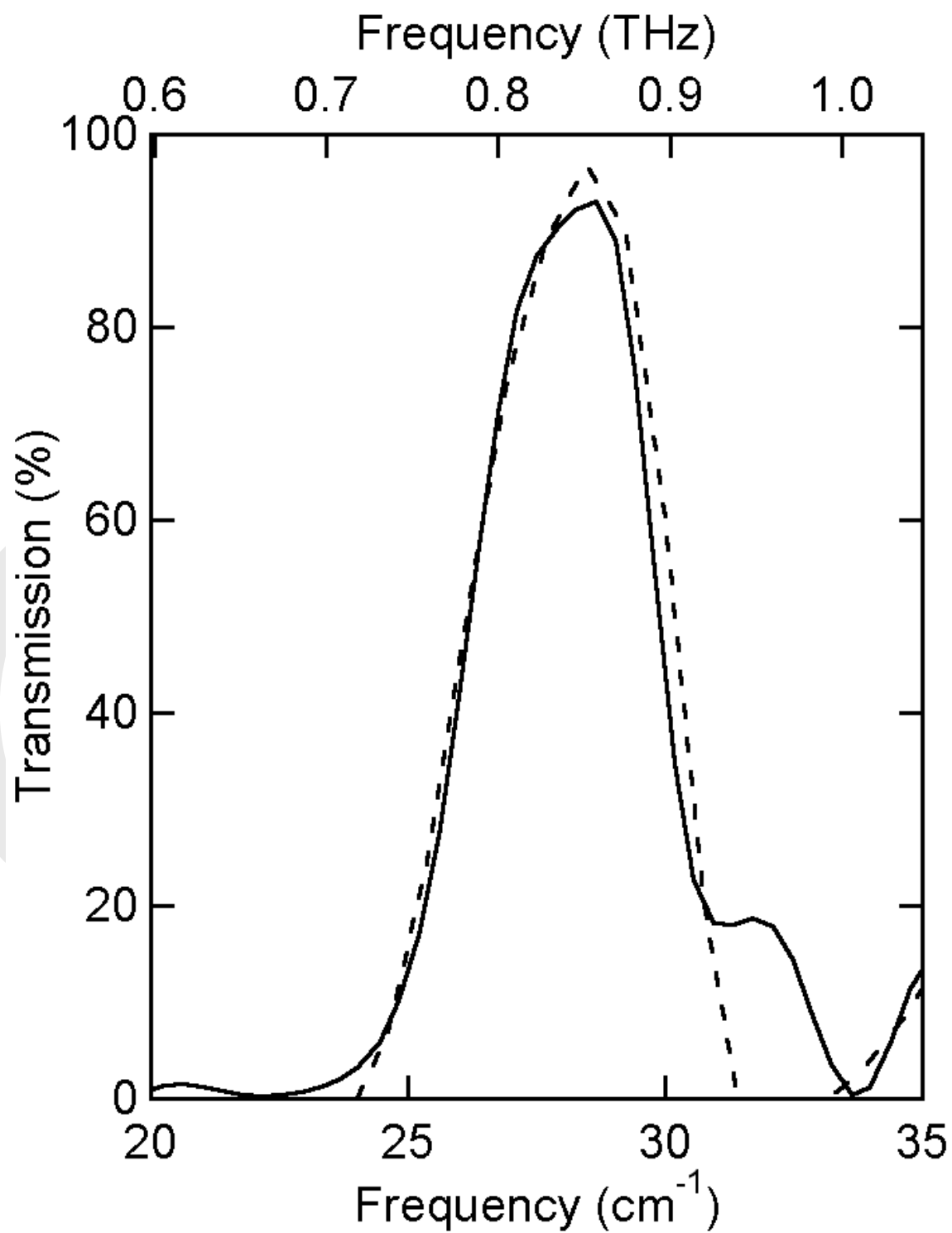


Figure 5.

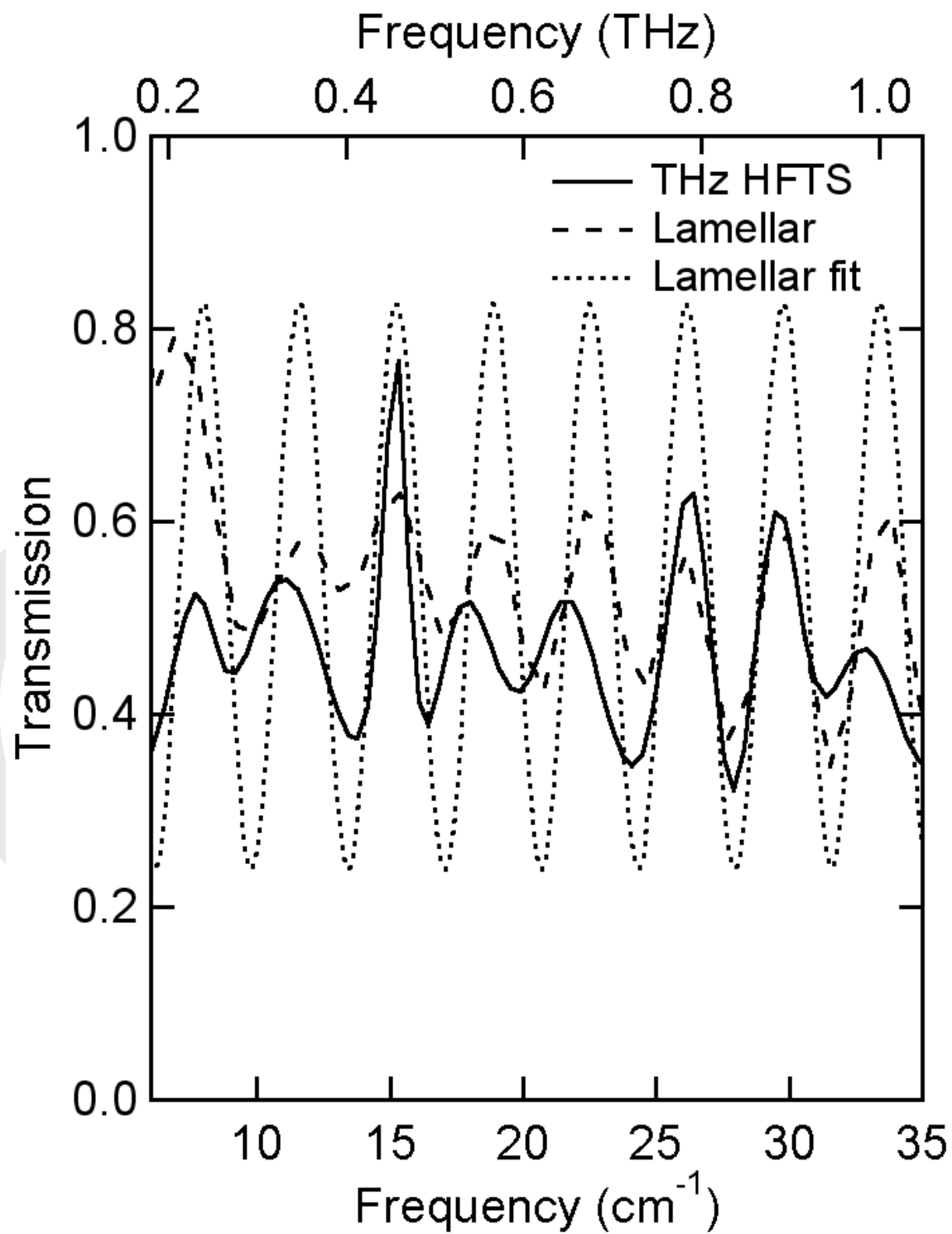


Figure 6.

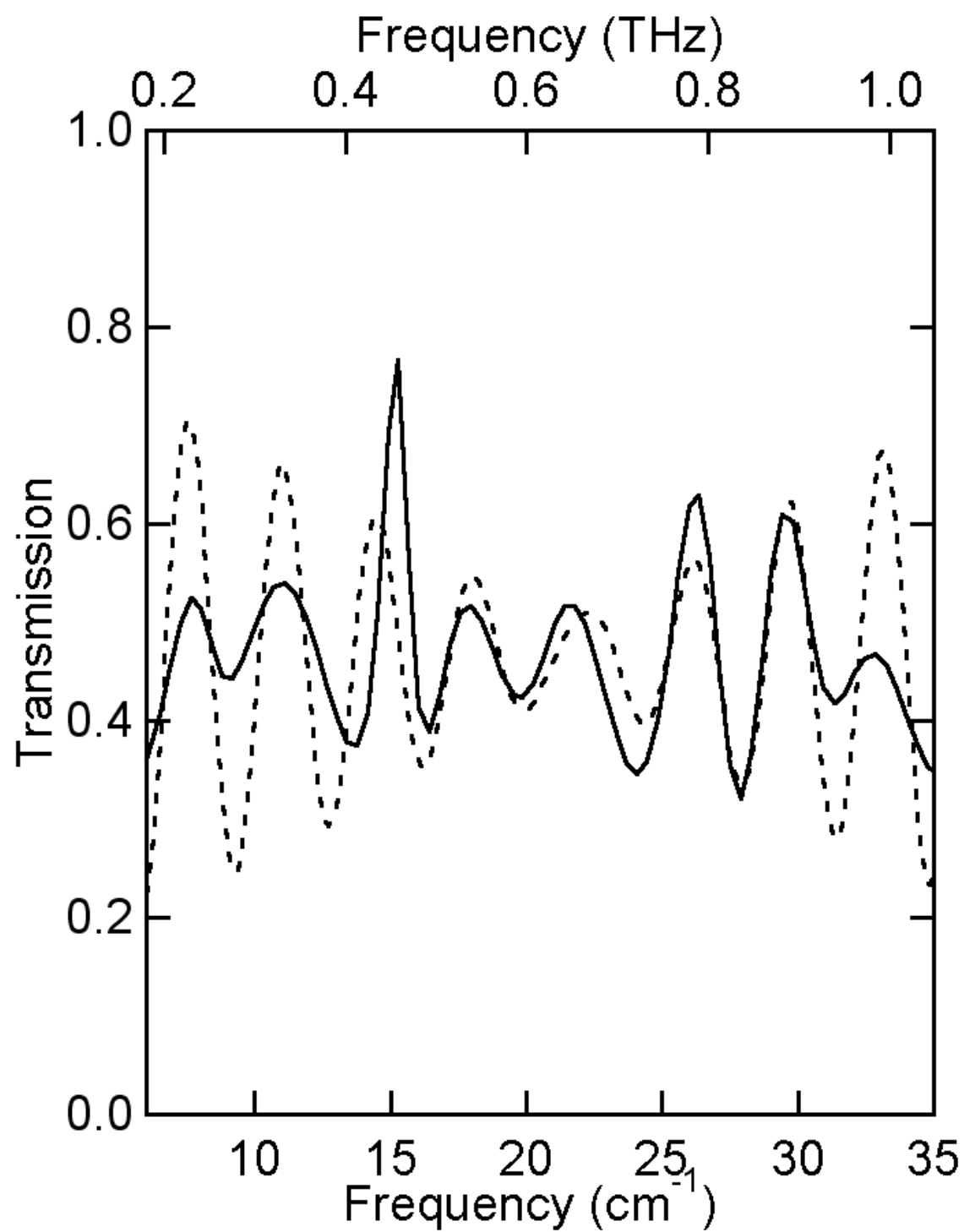


Figure 7.